Materials Science in Semiconductor Processing 39 (2015) 377–383

Contents lists available at ScienceDirect

Materials Science in Semiconductor Processing

journal homepage: www.elsevier.com/locate/mssp

Characterization of the MgO/$GaSe_{0.5}S_{0.5}$ heterojunction designed for visible light communications

A.F. Qasrawi [a,b,*], S.E. Al Garni [c], N.M. Gasanly [d,e]

[a] Department of Physics, Arab-American University, Jenin, West Bank, Palestine
[b] Group of Physics, Faculty of Engineering, Atilim University, 06836 Ankara, Turkey
[c] Physics Department, Sciences Faculty for Girls, King Abdulaziz University, Jeddah, Saudi Arabia
[d] Department of Physics, Middle East Technical University, 06800 Ankara, Turkey
[e] Virtual International Scientific Research Centre, Baku State University, 1148 Baku, Azerbaijan

ARTICLE INFO

Keywords:
Optical materials
Heterojunction
Optical spectroscopy
Dielectric properties

ABSTRACT

In this study an optoelectronic design is reported and characterized. The device is made of p-type MgO solved in sodium silicate binder and n-type $GaSe_{0.5}S_{0.5}$ heterojunction. It is described by means of X-ray diffraction, optical absorption and reflection in the incident light wavelength range of 190–1100 nm and by means of dark and 406 nm laser excited current (I)–voltage (V) characteristics. The optical reflectance was also measured as a function of angle of incidence of light in the range of 35–80°. The structural analysis revealed no change in the existing phases of the device composers. In addition, it was observed that for pure sodium silicate and for a 67% content of MgO solved in sodium silicate binder (33%), the heterojunction exhibits a valence band shift of 0.40 and 0.70 eV, respectively. The painting of MgO improved the light absorbability significantly. On the other hand, the angle-dependent reflectance measurements on the crystal displayed a Brewster condition at 70°. The MgO/ $GaSe_{0.5}S_{0.5}$ heterojunction exhibited no Brewster condition when irradiated from the MgO side. Moreover, for the crystal and the MgO/ $GaSe_{0.5}S_{0.5}$ heterojunction, the dielectric spectral analysis revealed a pronounced increase in the quality factor of the device. The I–V characteristics of the device revealed typical optoelectronic properties with high photo-response that could amplify the dark current 24 times when irradiated with 5 mW power laser light. The structural, optical, dielectric and electrical features of the MgO/$GaSe_{0.5}S_{0.5}$ heterojunction nominate it for use in visible light communication technology.

1. Introduction

Visible light communication (VLC) technology, which gets use of the free light spectrum have been shown as a good solution to many problems that arises from radio frequency and microwave communication tools [1–3]. In the VLC technology, the optical signal bandwidth can exceed 350 THz. In addition, the spatial confinement of light beams is reported to provide high security through preventing the interception or the eavesdropping. Moreover, with this recently developed communication tool the signal–to noise ratio is very high due to the brightness of light and the short distance between the emitter and receiver. The VLC transmission technology, which benefits from cheap light sources like leds to transmit broadband data streams, can be applied to the distribution of high-definition video streaming. It can also be employed for two

* Corresponding author at: Department of Physics, Arab-American University, Jenin, West Bank, Palestine. Tel.: +970 599379412; fax: +970 42510817.
E-mail addresses: atef.qasrawi@atilim.edu.tr, atef.qasrawi@aauj.edu (A.F. Qasrawi).

http://dx.doi.org/10.1016/j.mssp.2015.05.030
1369-8001/

way communication systems that cover the whole range from internet access to video conferencing [4].

One important component of the VLC technology is the photosensor that is used to convert light signal into electrical one. The conversion depends on the absorption level of the incident light signal. In addition, the transmitted and reflected light beams play role in this process. The design of the photosensor determines which light signals are to be absorbed or rejected [5–8]. In addition to the optical properties of the photodetector, the dark electrical current of the device play vital role in photosensing. Particularly, keeping the dark current at minimum increases the photo responsivity of the optical device. This can be obtained by constructing a back to back Schottky device or adding a dielectric layer around the active area to reduce the leakage currents and to ensure a low parasitic capacitance of the contact pad.

In our previous works we have used the boron nitride (BN) and MgO as dielectric layers that behave as an optical window for Ge and InSe photosensitive layers [7,8]. In addition, a back to back Schottky device which was made of carbon-$GaSe_{0.5}S_{0.5}$-carbon was characterized and observed to display a photosensitivity of 2.1×10^3[9]. The very high photosensitivity of these crystals and the effectiveness of the MgO as optical window, which reduces the reflectivity from the surface of the active layer, motivated us, here in this work, to design a new type of heterojunction that connect the active layer of the MSM device to the dielectric layer (MgO). The heterojunction structure, optical and electrical properties will be investigated. The possible range of spectral response will be explored prior to use these devices in VLC technology.

2. Experimental details

$GaSe_{0.5}S_{0.5}$ semiconductor polycrystals were synthesized using high-purity elements taken in stoichiometric proportions. Gallium (Aldrich cat. no. 263273), selenium (Aldrich cat. no. 204307) and sulfur (Fluka cat. no. 84680) were of 99.999% purity. The single crystals were grown by the Bridgman method from resultant polycrystalline ingots in evacuated (10^{-5} Torr) silica tubes (10 mm in diameter and about 55 cm in length) with a tip at the bottom in our crystal growth laboratory. No seed crystal was used. After evacuation and sealing off, the tube was introduced into the upper zone of a vertical two-zone growth furnace. The temperatures in the upper and lower zones were about 1000 and 650 °C. The temperature gradient between the zones was 30 °C cm^{-1}. After homogenizing the melt for 2 h, the tube was lowered through the gradient zone at a rate of 0.5 mm/h. Then the tube was pulled to the cold zone at the same rate, and the grown crystal was homogenized at 650 °C for 50 h. After that, the temperature of the cold zone was lowered to 400 °C and then the furnace was shut off. The resulting ingot was 8.5 mm, 35 cm and 13 g in diameter, length and mass, respectively. It was also air/moister stable. The crystals (orange in color) showed good optical quality and were easily cleaved along the planes that are perpendicular to the *c*-axis of the crystal. The final ingot exhibited monocrystalline nature. The samples selected for the measurements were taken from the middle part of the ingot. The n-type $GaSe_{0.5}S_{0.5}$ crystals were used as substrate for the p-type MgO layer. The cleaved crystal layers were restricted to be of $\sim d = 1.0$ μm thick. The MgO paste, which was prepared by solving the MgO nano-powders (Alfa Aeser 99.99%) in a silicate binder (SiO_2:Na_2O_2:CO3) was poured carefully on the surface of the crystals. Then it was vibrated and trembled continuously for few minutes to guarantee the homogeneous distribution of the MgO film. Although it is possible to obtain very thin layers of MgO paste down to ~1–2 μm, the homogeneous distribution of the layer which was observed microscopically, appears for layers of ~10 μm

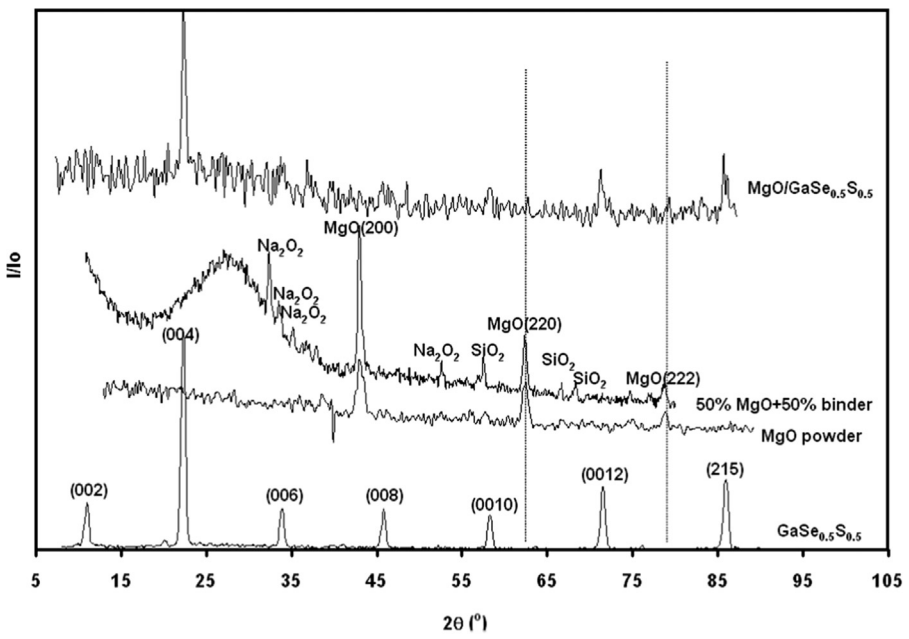

Fig. 1. The X-ray diffraction for the $GaSe_{0.5}S_{0.5}$ thin crystal, the MgO powder, the MgO powder solved in binder and the MgO/$GaSe_{0.5}S_{0.5}$ heterojunction.

thick. The studied MgO layer thickness was 12.6 μm. The X-ray diffraction was recorded using Rigaku Ultima IV. The current–voltage characteristics were recorded using Keithley 230 voltage source and Keithley 6485 picoammeter. The optical reflectance was measured as a function of angle of incidence in the range of 35–80° using PIKE VEE MAX II Reflectometer. The reflectance and transmittance were recoded in the incident wavelength range of 190–1100 nm. Laser excitations were actualized using a 406 nm Thor-Lab led laser light.

3. Results and discussion

In order to check the effect of the viscous liquid MgO paint on the cleaved crystal layer, the X-ray diffraction patterns (XRD) of the thin crystal before and after the painting of MgO were recorded. The XRD patterns, which are displayed in Fig. 1, relate to the MgO powder before solving it in the binder, the solved MgO in the binder, the cleaved $GaSe_{0.5}S_{0.5}$ crystal layer and for the MgO/$GaSe_{0.5}S_{0.5}$ double layer. The analysis of the data (using "TREOR 92" software) which is shown in the figure, indicated that the $GaSe_{0.5}S_{0.5}$ thin crystals are of hexagonal type of structure which are best oriented in the (004) direction and exhibit lattice parameters of $a=0.3671$ nm and $c=1.5719$ nm. On the other hand, the XRD patterns for the MgO powders displayed a cubic type of structure with unit cell lattice parameter of 4.203 $\mathring{A}$. The latter results are consistent with the PDF card no.: 00-001-1235. The binder did reflect any X-ray diffraction pattern before mixing it with MgO. However, when it was mixed with MgO, the XRD patterns of the mixture (50% MgO: 50% binder), which are shown in the figure, indicated all the MgO reflection peaks in addition to some minor peaks that relate to SiO_2 (PDF card no.:00-001-0378) and Na_2O_2. (PDF card no.: 00-001-1105) For MgO content larger than 70% only the MgO peaks appeared indicating that the binder phase became less dominant compared to that of MgO.

The data displayed in Fig. 1 also shows the X-ray diffraction patterns of the double layer after painting the crystal with MgO (67% MgO, 33% binder) paint. The diffraction patterns of the $GaSe_{0.5}S_{0.5}$ thin crystals appeared again. The appearance of the XRD patterns of the crystals after the painting of MgO means that there were no structural changes that could have happened as a result of the double layer design (during liquid–solid interfacing). The MgO reflection peaks are not strongly (see dotted lines which are presented in Fig. 1) apparent probably due to the intensity of the X-ray beam which is reflected from the crystal surface or due to much noise that is associated with the four phase (Na_2O_2, SiO_2, MgO, and $GaSe_{0.5}S_{0.5}$) XRD patterns. It was also observed that increasing the MgO content above 70% up to 99% does not allow the appearance of the $GaSe_{0.5}S_{0.5}$ thin crystal peaks. This disappearance is ascribed to the density of the MgO in the liquid content that become more dominant.

Fig. 2(a) displays the results of the optical absorbance ($A=\alpha d$; α is the absorption coefficient) being recoded in the incident photon energy range of 1.1–4.2 eV for the $GaSe_{0.5}S_{0.5}$ thin crystal, the binder, the binder/$GaSe_{0.5}S_{0.5}$, the MgO (67%)+binder(33%) and the MgO/$GaSe_{0.5}S_{0.5}$ double layer. The MgO/$GaSe_{0.5}S_{0.5}$ means that the 67% MgO is solved in 33% binder and then painted on the $GaSe_{0.5}S_{0.5}$ crystal surface. The presented absorbance spectral curves indicated interesting characteristics that are presented by the absorption level and absorption edge. For the samples under investigation the absorbance exhibits sharp decrease with decreasing incident photon energy. In general, below the absorption edge, the binder and the thin crystal are non-absorbing materials for all incident photon energies less than 3.40 and 2.36 eV, respectively. When the $GaSe_{0.5}S_{0.5}$ crystal is painted with the transparent paint only, the absorption edge shifted to 3.32 eV and the absorption level of the crystal increased five times. When the binder was mixed with 67% MgO the absorption level increased eleven times and no growth or decay as a response to photon energy was observed. This behavior appeared as a result of the inability to measure the sharp absorption region of MgO which is near its energy band gap 7.8 eV (due to instrumental limitations). Interfacing the crystal with MgO and binder mixture significantly increase the absorption level of the crystal by eleven times. In addition the absorption edge of the double layer now appeared at 2.19 eV. Assuming the validity of the relation $(AE)^2 \propto (E-E_g)$ and plotting the $(AE)^2$versus E, it is possible to determine the direct allowed transitions energy band gap of the samples. The energy band gaps of the binder and the $GaSe_{0.5}S_{0.5}$ crystal are 3.9 eV and 2.55 eV, respectively. Mixing the 67% MgO powder in 33% binder, reveal unmeasurable energy band gap due to instrumentation limitation. The energy band gap of the MgO/$GaSe_{0.5}S_{0.5}$ double layer is found to be 1.85 eV. When the same measurements are repeated for the binder – $GaSe_{0.5}S_{0.5}$ crystal double layer, the energy band gap exhibited value of 2.15 eV. The latter is reported to allow the comparison with the MgO effect. The valence band edge of the $GaSe_{0.5}S_{0.5}$ crystal shifts $(\Delta E_v = E_g(GaSe_{0.5}S_{0.5}) - E_g(MgO/GaSe_{0.5}S_{0.5})$ by 0.70 eV when the surface of the crystal is covered with MgO paste and by 0.40 eV when the $GaSe_{0.5}S_{0.5}$ crystal is covered with binder only.

The optical energy band gap of the crystal is comparable to those previously determined as 2.28 eV for a 125 μm thick $GaSe_{0.6}S_{0.4}$ crystal. It also coincides with that reported as 2.55 eV for $GaSe_{0.5}S_{0.5}$ crystal [10,11]. The energy band gap determined for the binder is also consistent with the value reported as 3.96 eV for sodium silicate glasses [12]. The mixing of the MgO with the binder increased the absorbability, but because the MgO is transparent in the measured spectral region (190–1100 nm), determining of the energy band gap for these films is not possible. The valence band shift associated with the double layer created from the binder or the binder–MgO mixture with the $GaSe_{0.5}S_{0.5}$ thin crystal is acceptable for the design of thin film transistors where a gap difference of 0.5–1.0 eV is needed. The binder/$GaSe_{0.5}S_{0.5}$ interface with the 0.40 eV shift is attractive for the design of point contact devices such as Schottky solar cells, resonant tunneling diodes and quantum dots [13,14]. This shift in the valence band of the $GaSe_{0.5}S_{0.5}$ crystal due to the MgO or binder interfacing could be assigned to the lattice mismatch at the interface of the heterojunction in addition to the defects that arise from

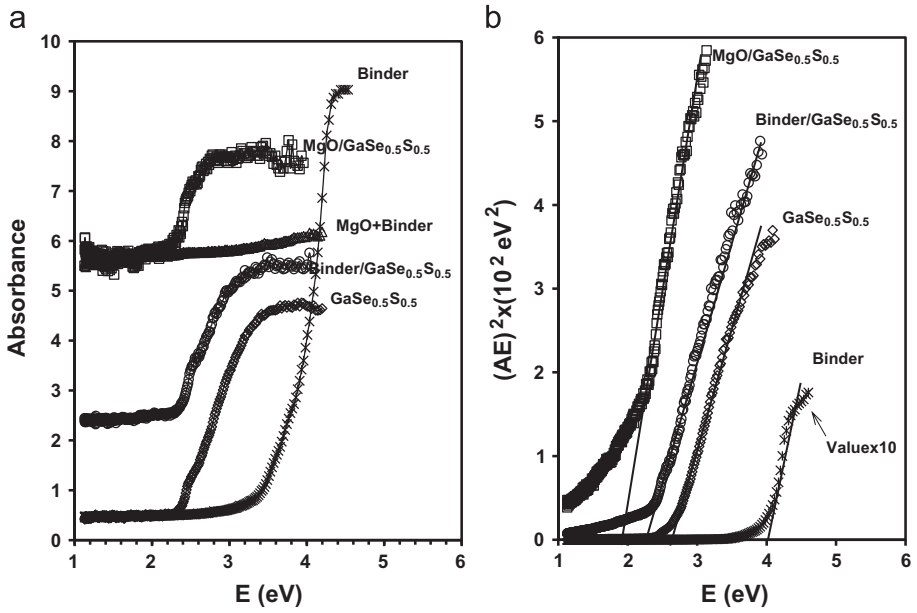

Fig. 2. (a) the absorbance spectra for the $GaSe_{0.5}S_{0.5}$ thin crystal, for the sodium silicate binder, MgO solved in binder and for the MgO/$GaSe_{0.5}S_{0.5}$ heterojunction. (b) the $(AE)^2-E$ dependence.

the impurities and incomplete bonds. The 0.70 eV value of shift, which was observed for the MgO/$GaSe_{0.5}S_{0.5}$ heterojunction, is mainly ascribed to the lattice mismatch between the hexagonal (004) oriented $GaSe_{0.5}S_{0.5}$ thin crystal and the (200) oriented cubic MgO as was shown in Fig. 1. The 0.70 eV value is much larger than we have previously determined as 0.23 eV for the MgO/Ga_4Se_3S heterojunction [14].

It is important to notice that, the reason for preferring the 67% MgO to 33% binder paste in this work compared to our previously reported in ref. 14 when a 99% MgO is solved in the 1% binder is that the increase of the binder content makes the top layer harder and the surface of the heterojunction smoother.

Fig. 3(a) and (b) illustrates the reflectance spectra for the $GaSe_{0.5}S_{0.5}$ crystal and the MgO/ $GaSe_{0.5}S_{0.5}$ heterojunction, being recorded at various angles of incidence of light in the range of 35–80°. In general, the reflection spectra exhibit the same characteristics at each angle of measurement. The effects of angle of incidence (θ_i) on the reflection coefficient (R) of the crystal and on the heterojunction are better presented in Fig. 3(c) and (d), for three particular wavelengths (400, 800 and 1000 nm), respectively. These three wavelengths are selected as they related to the famously used light emitting diodes in visible light technology. The reflection coefficient (Fig. 3(c)) of the thin crystals slightly decreases with increasing angle of incidence up to 50°. For higher angles, values sharply falls approaching zero value at θ_i of 70°. This value relates to a Brewster condition in which the light exhibits total internal reflectance at this angle of incidence. This strange behavior of the $GaSe_{0.5}S_{0.5}$ thin crystals, which is similar to the Ga_4Se_3S crystal, was previously discussed [14] and was ascribed to the crystalline nature of these materials. The crystal is composed of very thin layers attached through weak bonding forces.

The data of $R-\theta_i$ variation which are presented in Fig. 3 (d) relate to the heterojunction as being recorded from the MgO side. The reflectivity of the $GaSe_{0.5}S_{0.5}$ sharply decreases by ~97% by the painting of MgO. This explains the reason for the large increase in the absorbability of the heterojunction (Fig. 2(a)). The reduction of the reflectance via heterojunction design has an extra advantage as it enhances the internal quantum efficiency, when this pn junction is used as a solar energy converter or as it converts the light to electrical signal.

Fig. 4(a) and (b) shows the real and imaginary parts of dielectric spectra for the $GaSe_{0.5}S_{0.5}$ and the MgO/ $GaSe_{0.5}S_{0.5}$ heterojunction, respectively. The dielectric constant is determined using the same method which was previously described in our works [7,8]. One important feature of the real dielectric constant of the thin crystal is that it exhibits a resonance peak at a frequency of 519 THz. Another feature is that for incident wave frequency less than 350 THz, the ε_r sharply increases with decreasing frequency reaching a value of 20 at 270 THz. On the one hand, the imaginary part of the dielectric constant (ε_{im}) whose value is relatively low compared to ε_r, increased with decreasing frequency down to 730 THz. Below which, it sharply falls from a value of 1.1 reaching ~0.01 near 270 THz. This variation significantly affects the quality factor (Q) for the thin crystal which is defined as the inverse of the loss tangent ($\tan(\delta)$). The incident light frequency dependent quality factor of the thin crystal is presented in Fig. 4(c). The Q values gain meaning for frequencies less than 590 THz. Above this value, the crystal is not able to store or resonate any incident electromagnetic signal, as the energy dispersion above 590 THz is very high. Thus, the $GaSe_{0.5}S_{0.5}$ crystals are effective for use in VLC technology, provided that the incident light exhibit wavelength greater than 508 nm (green light). On the other hand, the MgO/ $GaSe_{0.5}S_{0.5}$ heterojunction

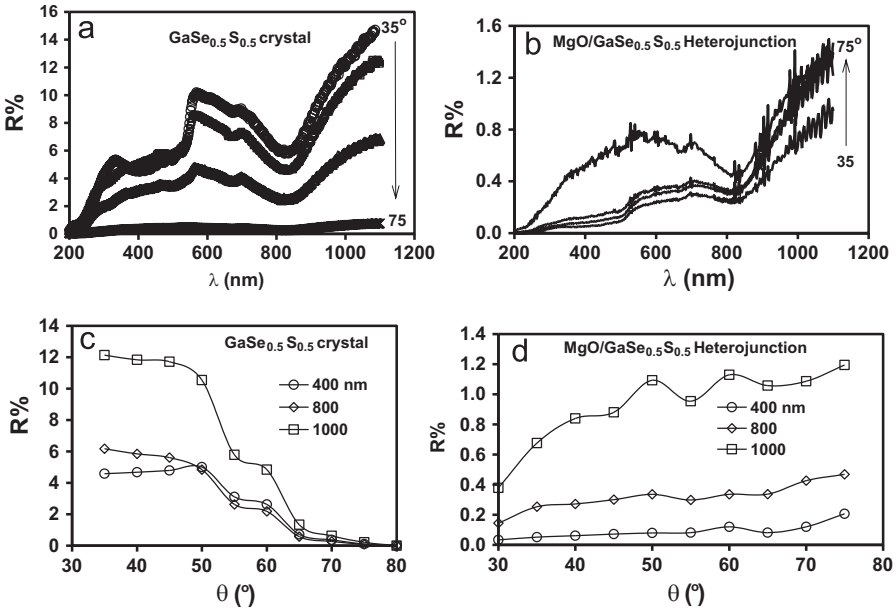

Fig. 3. The reflection spectra at various angles of incidence for (a) the $GaSe_{0.5}S_{0.5}$ thin crystal and (b) for the $MgO/GaSe_{0.5}S_{0.5}$ heterojunction. (c) and (d) represents the $R-\theta_i$ dependence for the $GaSe_{0.5}S_{0.5}$ thin crystal and the heterojunction, respectively.

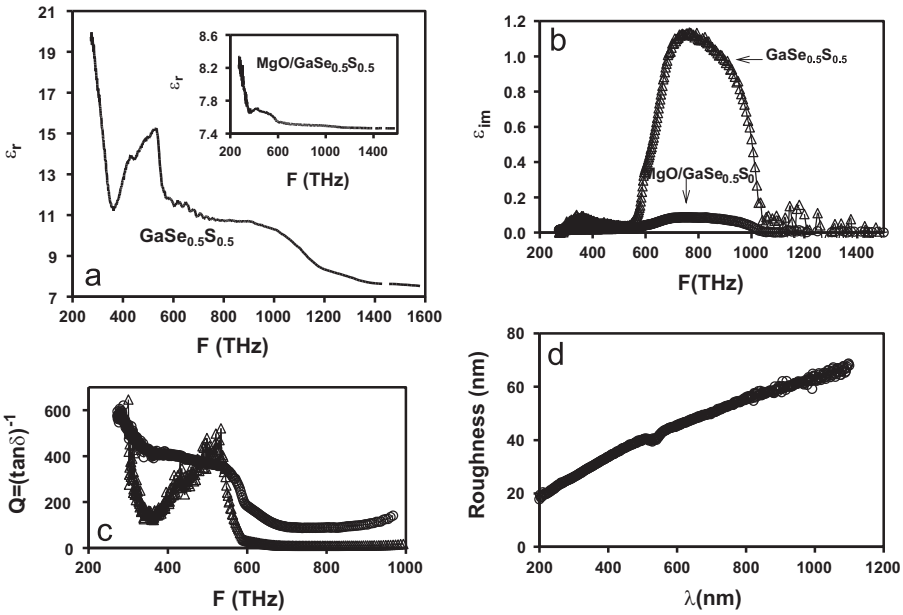

Fig. 4. The real dielectric (a) and imaginary dielectric (b) and the quality factor (c) spectra for the $GaSe_{0.5}S_{0.5}$ thin crystal and the heterojunction and (d) is the roughness spectral analysis for the heterojunction.

reflected a sharp decrease in the values of the dielectric constant compared to the thin crystal. The general features of the real part of the dielectric constant (inset of Fig. 4(a)) did not change after the painting of MgO. However, the resonance peak now appears at 406 THz and becomes less pronounced. The imaginary part of the dielectric constant for the heterojunction which is displayed in Fig. 4(b) is relatively low compared to that of the crystal. This sharp decay in the values caused a remarkable improvement in the quality factor of the device. The Q values, which appear in Fig. 4(c), indicate that the ability of heterojunction to store electromagnetic signals start at 1500 THz instead of 590 THz for the crystal alone. It becomes more pronounced when it reaches the IR region of the spectrum.

The sharp decrease in the values of the dielectric constant as a result of the MgO painting could be ascribed to the increase in the free carrier density that is associated with the adding of MgO. The MgO crystals exhibit a free hole density of $\sim 10^{15}\ cm^{-3}$ [14] compared to the crystals whose free electron density is $\sim 10^{12}\ cm^{-3}$ [9].

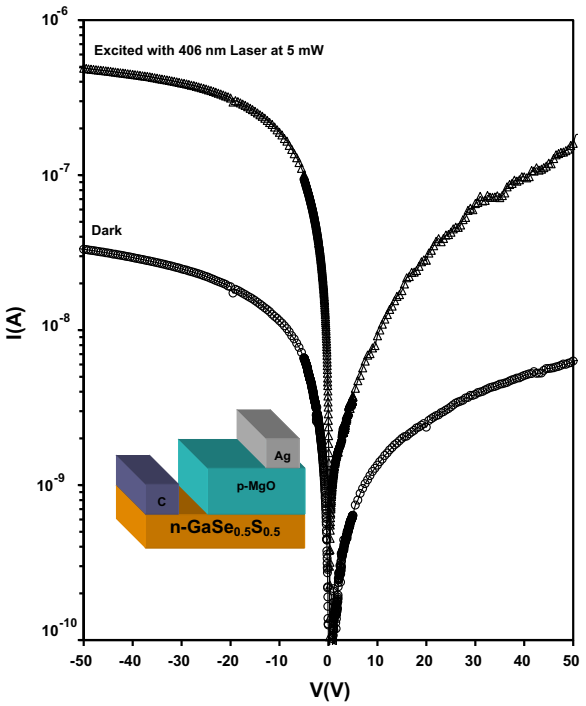

Fig. 5. The *I–V* characteristics of the Ag/MgO/$GaSe_{0.5}S_{0.5}$/C devices in the dark and under photoexcitation.

The root mean square (RMS) roughness (σ) of the double layer film surface after the painting of MgO on the $GaSe_{0.5}S_{0.5}$ thin crystal are determined by the Nevot-Croce approach [15]. The roughness of the surface are determined using the measured reflectivity data in which the reflection coefficient is in accordance with the equation

$$R = R_o \exp\left(-n_1 n_2 \sin\theta_1 \sin\theta_2 \left(\frac{4\pi\sigma}{\lambda}\right)^2\right) \quad (1)$$

Here, R_o, n_1, n_2, $\theta_1$and θ_2 refer to the reflectance from the smooth surface which is the surface of the $GaSe_{0.5}S_{0.5}$ thin crystal, the refractive index ($n=\sqrt{\varepsilon}$) of the MgO layer, the refractive index of the $GaSe_{0.5}S_{0.5}$ layer, the angle of incidence of light onto the MgO and the angle of incidence after refraction from the MgO layer, respectively. Using the reflectivity data which is presented in Fig. 3(a) and the dielectric constant data which is presented in Fig. 4 to obtain the refractive indices of the layers, the upper surface roughness were calculated and presented in Fig. 4(d). As it is readable, the roughness values of the MgO film oscillate between 18 and 68 nm. The surface roughness are steadily increasing with increasing wavelength reaching a maximum value of 68 nm at $\lambda=1100$ nm. This represents 5.4% of the measured thickness of the top double layer indicating the films are smooth enough to be used in the design of optical devices.

In order to test the device applicability in VLC technology, the MgO/$GaSe_{0.5}S_{0.5}$ devices was contacted with carbon on the $GaSe_{0.5}S_{0.5}$ side and with Ag metal on the MgO side. The geometrical design of the device is shown in the inset of Fig. 5. The carbon is used to force the creation of a Schottky barrier at the crystal side [9]. These Schottky barrier is a n-type majority carrier device under forward biasing conditions. The MgO side of the device is also contacted to Ag metal as it creates another Schottky device with p-type majority carriers [16]. The mid-structure (MgO/$GaSe_{0.5}S_{0.5}$) represents a pn junction. The pn junction is known as minority carrier devices. The recorded current–voltage characteristics of the device in the dark and under the excitation of a 5.0 mW laser light are presented in Fig. 5. The selected laser generates light of wavelength of 406 nm. As it is readable from the figure, the reverse current is larger than the forward one. This behavior is due to the design of the device in which one of the metal contacts is attached to a wide energy band gap (MgO) and the other to narrower energy band gap. Thus, the forward biased conduction is governed by thermionic emission of charge carriers over the Schottky (C/$GaSe_{0.5}S_{0.5}$) barrier height and the reverse biased conduction mechanism is governed by the electric field assisted thermionic emission or tunneling of charge carriers through the very large energy barriers at Ag/MgO side [9,17]. The laser excitation of the device enlarged the current significantly. As, for example, at reverse biasing voltage of 10 V, the light to the dark current ratio is 17; this value has increased to 23 at ~30 V. The performance of the device is promising as it indicates its applicability of converting light signals to electrical ones.

4. Conclusions

In this article, we have discussed the optimum design of MgO/$GaSe_{0.5}S_{0.5}$ heterojunction. The possible structural, optical and electrical modifications that are associated with the design of the heterojunction are investigated. The structural analysis has shown that the crystal is not affected by the painting of MgO on its surface. In addition, the optical analysis reflected a wide range of photoresponse that extends from blue light to near IR. Wide tunability of valence band shift is possible via altering the MgO content in the paint. In addition, a large improvement in the absorbability and electromagnetic energy storability is observed. These features combined to the photoresponse of the current–voltage characteristics under laser excitation are promising results that suggest the applicability of these devices in optoelectronics.

Acknowledgments

The scientific research council at the ministry of higher education of the state of Palestine is acknowledged and thanked for their support to the physics laboratories at the Arab-American University through the project titled "Design and Characterization of MgO/$GaSe_{0.5}S_{0.5}$ Multifunctional Resonant Microwave Optoelectronic Sensors" and coded 2/1/2013.

References

[1] X. Bao, G. Yu, J. Dai, X. Zhu, Wireless networks, In press, (2015), http://dx.doi.org/10.1007/s11276-015-0889-0.
[2] C.W. Chow, Ch.H. Yeh, Curr. Trends Opt. Photon. 129 (2015) 107–121.
[3] F. Miramirkhani, M. Uysal, E. Panayirci, Proc. SPIE 9387 (2015) 93870Q, http://dx.doi.org/10.1117/12.2077565.
[4] J. He, R.A. Norwood, M. Brandt-Pearce, I.B. Djordjevic, M. Cvijetic, S. Subramaniam, R. Himmelhuber, C. Reynolds, P. Blanche, B. Lynn, N. Peyghambarian, Comp. Electr. Eng. 40 (2014) 216–240.
[5] B. Arredondo, B. Romero, J. Sánchez Pena, A. Fernández-Pacheco, E. Alonso, R. Vergaz, C. de Dios, Sensors 13 (2013) 12266–12276.
[6] V. Silva, P. Louro, M.A. Vieira, I. Rodrigues, M. Vieira, Sens. Transducer 185 (2015) 78–83.
[7] S.E. Al Garnia, A.F. Qasrawi, Mater. Sci. Semicond. Process. 31 (2015) 678–683.
[8] T.S. Kayed, A.F. Qasrawi, K.A. Elsayed, Phys. Status Solidi B 252 (2015) 621–625.
[9] H.K. Khanfar, A.F. Qasrawi, N.M. Gasanly, Sens. J. 15 (2015) 2269–2273.
[10] V. Petrov, V.L. Panyutin, A. Tyazhev, G. Marchev, A.I. Zagumennyi, F. Rotermund, F. Noack, K. Miyata, L.D. Iskhakova, A.F. Zerrouk, Laser Phys. 21 (2011) 774–781.
[11] A.M. Mancini, A. Rizzo, R. Girlanda, G. Guizzetti, L. Nosenzo, E. Doni, E. Reguzzoni, IL. Nuovo Cimento, 1D (1982) 751–776.
[12] V. Kumar, S. Tyagi, K. Singh, Indian J. Pure Appl. Phys. 50 (2012) 335–338.
[13] M. Grundmann, The Physics of Semiconductors: An Introduction Including Nanophysics and applications, 2nd ed. Springer, New York, 2010.
[14] A.F. Qasrawi, M.M. Abd-Alrazq, N.M. Gasanly, J. Alloy. Compd. 583 (2014) 180–185.
[15] D.K.G. De Boer, Phys. Rev. B 49 (1994) 5817.
[16] T. Jaouen, G. Jézéquel, G. Delhaye, B. Lépine, P. Turban, P. Schieffer, Appl. Phys. Lett. 97 (2010) 232104.
[17] T. Kado, Appl. Phys. Lett. 80 (2002) 3382.